Chalcogenide Fabry–Perot Fiber Tunable Filter

Kaixuan Zhang, *Member, IEEE*, Yves-Alain Peter, *Senior Member, IEEE*, and Martin Rochette, *Senior Member, IEEE*

***Abstract*— We demonstrate the first mid-infrared compatible all-fiber Fabry–Perot filter. It consists of chalcogenide fibers terminated with high-reflective coatings made of germanium and calcium fluoride. In addition to the transmission compatibility with mid-infrared wavelength, the filter has both tunability and free spectral range >350 nm as well as a finesse of 27. To demonstrate the application of the filter, a thulium-doped fiber laser is built and shows continuous tunability from 1.835 to 1.920 μm.**

***Index Terms*— Chalcogenide glass fiber, high-reflective thin-films, Fabry-Perot, optical fiber filter, mid-infrared tunable laser.**

I. Introduction

MID-INFRARED (MIR) light in the wavelength range of 2-12 μm is attractive for both research and technology applications. Strong characteristic molecular absorptions in the MIR are most useful to chemical sensing [1], [2]. Free-space communications utilize the transparent windows of earth's atmosphere at wavelength 3-5 μm and 8-13 μm [3]. Some wavelengths in the MIR are also desirable for their high ablation efficiency and small collateral damage when treating biological soft tissues [4]. With an aim to build robust optical sources operating in the MIR wavelength range, an all-fiber approach is most desirable to bring the advantages of compactness, compatibility with other fiber components and operational stability in hostile environments. Thus, building block components such as all-fiber filters need to be designed for laser sources and other wavelength selective systems in the MIR range.

Several in-fiber optical filter technologies have been developed for telecommunications. Geng *et al.* [5] reported a tunable Fabry-Perot (FP) filter with high finesse and broad tunability from 1.85 μm to 2.15 μm, but limited by the transmission window of silica fiber. Lee *et al.* [6] demonstrated a fiber acousto-optic filter tunable from 1.53 μm to 1.62 μm and Bharathan *et al.* [7] demonstrated a Bragg-grating filter on ZBLAN fluoride fiber tunable from 2.850 μm to 2.887 μm. As an alternative to silica and fluoride glasses, chalcogenide glass fibers such as those based on As_2S_3 and As_2Se_3 are well known for their transparency up to 6.5 μm and 10 μm, respectively [8], [9]. Their unique optical properties [10] in the MIR wavelength range have already proven to be useful in applications such as fiber couplers [11], supercontinuum sources (SC) [12], [13] and amplifiers [14], [15]. Filters have also been proposed using chalcogenide glasses [16], [17]. Littler *et al.* [16] demonstrated a chalcogenide acousto-optic filter tunable over 235 nm around a central wavelength of 1.45 μm with a maximum sideband suppression of 9 dB, limited by the applied RF power. Ahmad and Rochette [17] reported a fiber Bragg-grating filter inscribed into chalcogenide wires with a tunability of ~50 nm around a central wavelength of 1.55 μm. The lack of broadly tunable filters compatible with the MIR range motivates the fabrication of a MIR compatible, widely tunable, all-fiber filter with large sideband suppression ratio.

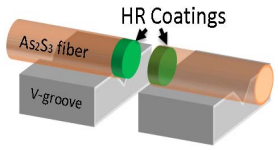

Fig. 1. Fabry-Perot tunable filter structure. V groove supports are resting on 5-axis translation and rotation stages.

In this letter, we present the first all-fiber Fabry-Perot tunable filter (FFP-TF) compatible with the MIR range. The filter is made of chalcogenide fibers coated with high-reflective (HR) thin-films made from alternate layer of germanium (Ge) and calcium fluoride (CaF_2). This thin-film structure is expected to be compatible with the whole MIR band. As a proof of concept to demonstrate the potential application of this FFP-TF, an all-fiber laser is assembled and shows tunability in the spectral range of 1.9 μm.

II. Design and Fabrication

Figure 1 shows the schematic of FFP-TF. As_2S_3 fibers with core/cladding diameters of 6/170 μm provided by *CorActive High-Tech* are well polished as substrates for the deposition of dielectric materials. The thin-films with quarter-wavelength multilayer structure are designed to cover the spectral band of 1.1-2.8 μm. A FP cavity is formed by facing two HR coated chalcogenide fibers. Fiber alignment is achieved by adjusting two 5-axis translation/rotation stages and tuning is realized by changing the air gap distance between the two fibers.

Manuscript received August 29, 2018; revised October 2, 2018; accepted October 3, 2018. Date of publication October 9, 2018; date of current version November 20, 2018. This work was supported in part by CorActive High-Tech, in part by CMC Microsystems, in part by Natural Sciences and Engineering Research Council of Canada, and in part by Fonds de Recherche du Quebec-Nature et Technologies. *(Corresponding author: Kaixuan Zhang.)*

K. Zhang and M. Rochette are with the Department of Electrical and Computer Engineering, McGill University, Montréal, QC H3A 0E9, Canada (e-mail: kaixuan.zhang@mail.mcgill.ca; martin.rochette@mcgill.ca).

Y.-A. Peter is with the Department of Engineering Physics, Polytechnique Montréal, Montréal, QC H3C 3A7, Canada (e-mail: yves-alain.peter@polymtl.ca).

Color versions of one or more of the figures in this letter are available online at http://ieeexplore.ieee.org.

Digital Object Identifier 10.1109/LPT.2018.2874644

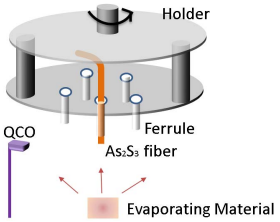

Fig. 2. Electron-beam evaporation system for thin film coating deposition. QCO, quartz crystal oscillator.

The choices of dielectric materials for HR coatings mainly depend on factors such as (1) refractive indices, (2) transparent wavelengths, (3) compatibility with other materials and (4) stability of the multilayer structure. The most common materials used for MIR thin-films are MgF_2, CaF_2, ZnS, ZnSe, TiO_2 and Ge [18]. We use CaF_2 as the low refractive index material with $n_L = 1.42$ at $\lambda = 2$ μm [19] because of its low tensile stress [20], and Ge as the high refractive index material with $n_H = 4.16$ at $\lambda = 2$ μm [21] to get large refractive index contrast. The high refractive index contrast between CaF_2 and Ge leads to stable HR coatings with less total thickness and broader reflection spectral bandwidth compared to other common materials used for IR thin-films.

To fabricate HR coatings, thin-films are deposited on fiber facets with quarter-wavelength thicknesses: $d_k = \frac{\lambda_0}{4n_k}$, where k is the layer number, n_k is the refractive index of k^{th} layer, and λ_0 is the designed central wavelength of the broadband reflection spectrum.

Coatings are fabricated with an electron-beam evaporation system because of its compatibility with a variety of materials and ease of operation. Before deposition of the multilayered thin-films, it is necessary to calibrate the crystal oscillator for *in situ* deposited thickness monitoring. For this purpose, single layers of CaF_2 and Ge are deposited on small pieces of silicon chip. Then the thickness and refractive index are fitted using an ellipsometer. The obtained refractive indices are subsequently used in a thin film reflectometry system to verify the layer thickness, and a surface profiler (Dektak 150) is also used to verify the thickness. During the calibration, the refractive index of CaF_2 is determined at $\sim$1.25 at a wavelength of 2 μm, with a gradient distribution spreading over a thickness of 100 nm. This phenomenon, also reported by Heavens and Smith [22], mainly comes from the porous structure of the CaF_2 thin-film. This gradient could be avoided using ion-assisted electron-beam evaporation system [23]. The measured refractive index of Ge is 4.1 at a wavelength of 2 μm and is uniform across the thin-film.

Figure 2 illustrates the schematic of the electron-beam evaporation chamber. Multilayered thin-films are deposited on polished chalcogenide fiber facets without temperature control of the substrates. One end of the fiber is kept on the holder and the other end goes through a ferrule to keep the fiber vertically oriented. The holder is rotating to improve deposition uniformity. Dielectric materials are heated and evaporated by an electron-beam and subsequently condensed on fiber facets. During deposition, thickness is monitored using the quartz crystal oscillator, and the chamber pressure is kept under 5×10^{-6} Torr. After deposition, no annealing process is applied.

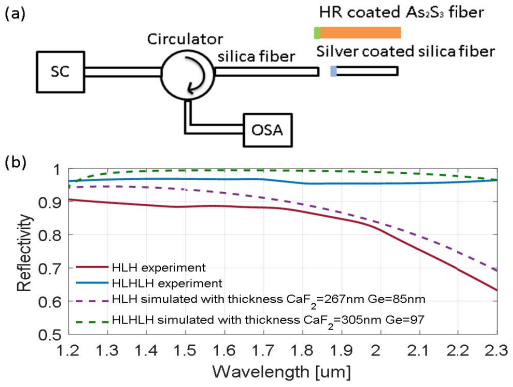

Fig. 3. (a) Schematic to measure the reflection spectrum of HR coatings. SC, supercontinuum source; OSA, optical spectrum analyzer. First tested with silver coated silica fiber, then tested with HR coated As_2S_3 fiber. (b) Measured and simulated reflection spectra of HR coatings with HLHLH and HLH layer structures. H, high refractive index; L, low refractive index.

The thickness accuracy of each layer is controlled within an error of 15 nm, which corresponds to the stability of the quartz crystal oscillator and the calibration procedure. The central wavelength of the HR coating is arbitrarily set to 1.6 μm in this experiment, resulting into a theoretical HR spectral range of 1.1-2.8 μm, and requiring layer thickness of 305 nm and 97 nm for CaF_2 and Ge, respectively. The deposition rate is set at 0.2 nm/s. HR coatings with alternate thin-film layers of "high-low-high" (HLH) and "HLHLH" materials are deposited on As_2S_3 fiber facets.

III. Characterization of Coatings

Figure 3a shows the HR coatings characterization setup, including a supercontinuum source (SC), an optical spectrum analyzer (OSA), and an optical circulator. A silica fiber coated with a 30 nm thick layer of silver serves as a reference mirror, providing a broadband reflectivity of 95% across the spectral range 1.3-2.5 μm. The reflection spectrum of As_2S_3 fiber coated with HR thin-films is then measured relative to the reference spectrum. The reflection spectrum of multilayer coating based on Gaussian beam propagation and matrix theory [27] is also simulated for comparison.

The reflection spectrum is theoretically expressed as:

$$R_{ref} = R_{silica} + \frac{T_{silica}^2 R_{Ag}}{1 - R_{silica} R_{Ag}} \quad (1)$$

$$R_{sample} = R_{silica} + \frac{T_{silica}^2 R_{HR}}{1 - R_{silica} R_{HR}} \quad (2)$$

Where R_{Ag} is the reflectivity of the silver coated silica fiber facet in air, R_{silica} and T_{silica} are the reflectivity and transmittance of silica fiber facet in air, and R_{HR} is the reflectivity of HR coated As_2S_3 fiber facet in air. R_{ref} and R_{sample} are reflectivities obtained at the OSA. when the R_{Ag} and R_{HR} >82.6%, the difference between R_{ref} and R_{Ag}, R_{sample} and R_{HR} is <0.1%. Regarding the reflectivity of the

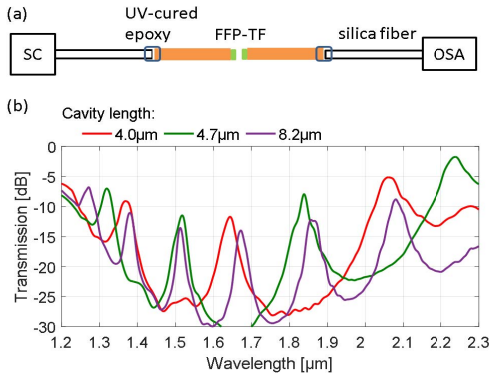

Fig. 4. (a) Schematic to measure the transmission spectrum of FFP-FT. SC, supercontinuum source; FFP-TF: fiber Fabry-Perot tunable filter; OSA, optical spectrum analyzer. (b) Measured transmission spectra of FFP-FT with different cavity length.

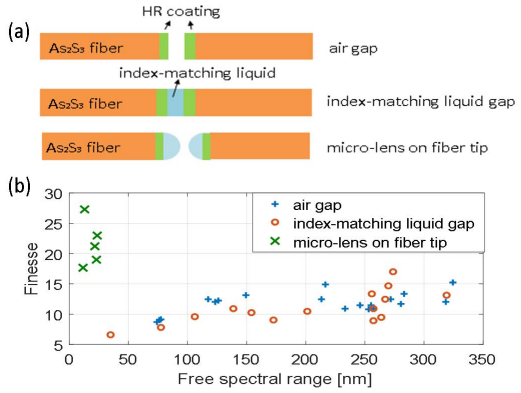

Fig. 5. (a) Schematics of FP cavity with gap formed by air, index-matching liquid and micro-lens. (b) Measured finesse versus free spectral range by different coupling methods.

fabricated HR coating and the silver layer, $R_{ref} \approx R_{Ag}$ and $R_{sample} \approx R_{HR}$.

Figure 3b shows the measured reflection spectra of the HR coatings on As_2S_3 fibers, from 1.2 μm to 2.3 μm. The short wavelength bound is limited by the operating wavelength range of the OSA and the upper wavelength bound is limited by the transmission window of silica fiber. The measured reflectivity of the HR coating with 5 thin-films is 96% and that with 3 thin-films is 90%. The central wavelength of the HR coating with 3 thin-films is shifted towards shorter wavelength of 1.3 μm due to reduced thicknesses. The surface roughness of the coating is measured using an atomic force microscopy and the RMS roughness of 10 nm is observed, with an expected impact to reduce the theoretical reflectivity ~4% [24], [25].

IV. Characterization of Filter and Laser

Figure 4a shows the characterization setup of FFP-TF. It consists of two chalcogenide fibers with HR coatings of 5 thin-film layers facing each other. Light from the SC is coupled through a silica fiber into the FP cavity and transmitted to the OSA through another silica fiber. UV-cured epoxy is applied to connect the silica fiber and As_2S_3 fiber with a coupling loss of ~2.5 dB. This loss includes 0.3 dB loss due to Fresnel reflection, 0.7 dB loss due to mode mismatch and 1.5 dB loss due to angular misalignment. Figure 4b shows the FP optical responses for different cavity lengths. Though the As_2S_3 fiber is designed to be single mode at wavelength >2 μm, no significant multimode interference is observed at the whole demonstration wavelength range from 1.2 μm to 2.3 μm. A free spectral range (FSR) of 350 nm with a finesse of 17 is obtained when the cavity length is ~4 μm. The finesse is limited by coupling loss at the cavity gap and can be increased to 27 with the use of micro lens on fiber tips, which are formed by liquid drops with a refractive index of 1.4715, as reported by Jiang and Tang [26]. The FSR is then limited to 25 nm because of the longer cavity length involved with the use of liquid drops. Figure 5a and 5b show the schematics of different coupling methods and the relationship between finesse and FSR. It appears that the finesse is not improved significantly when filling the gap with index-matching liquid (Cargille immersion liquid 5040).

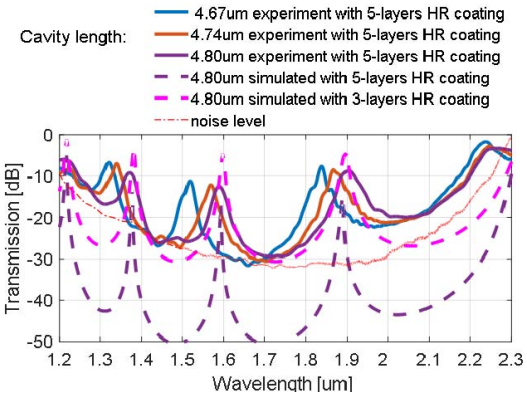

Fig. 6. Measured and simulated transmission spectra of FFP-TF within 0.2 μm variation of cavity length. 5-layer HR coating has HLHLH structure; 3-layer HR coating has HLH structure; H, high refractive index; L, low refractive index. Noise level is due to the sensitivity limit of OSA.

Figure 6 shows the FP transmission peaks that are continuously shifting by changing the cavity length. A tunable filter with FSR above 300 nm and a finesse of 15 is obtained. The FFT-TF has an insertion loss of 13 dB and an extinction ratio of 17 dB at the central wavelength. This wavelength-dependent loss and extinction ratio are attributed to the Gaussian free space propagation among two flat HR mirrors. A Gaussian beam propagation simulation result with a FP cavity consists of 5 thin-films HR coatings is shown in the dashed purple line, from which the insertion loss is ~16 dB. The simulation method for Gaussian beam propagating through the FFT-TF is described by St-Gelais *et al.* [27]. Mismatch in between experimental and theoretical spectra arises from experimental imperfections of the 5-layers HR coating combined with the proximity to the noise floor of the OSA.

Figure 7 illustrates the schematic of a thulium (Tm) doped all-fiber tunable laser assembled with the FFP-TF. Tm is chosen as the gain medium to make a proof of concept use of the FFP-TF. However, the same fiber filter cavity could serve with a gain medium such as Er-doped ZBLAN [12]

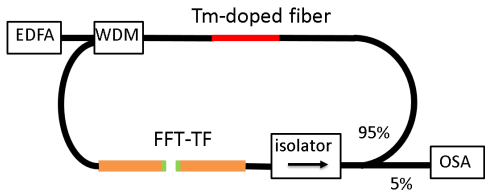

Fig. 7. Schematic of Tm-doped fiber tunable laser. EDFA, erbium-doped fiber amplifier; WDM, 1.55 μm/1.85 μm wavelength division multiplexer; FFT-TF, fiber Fabry-Perot tunable filter; OSA, optical spectrum analyzer.

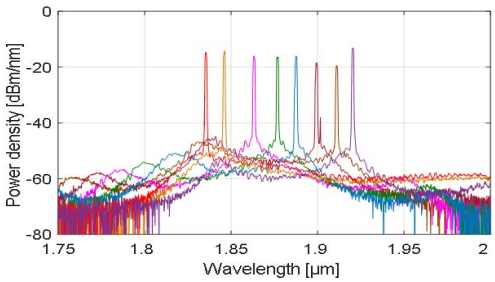

Fig. 8. Measured spectra of the Tm-doped fiber tunable laser.

to make a truly MIR tunable laser source. The 30 cm long Tm-doped fiber is pumped with a total of 1.5 W of amplified spontaneous emission (ASE) of an erbium-doped fiber amplifier (EDFA), via a 1.55 μm/1.85 μm wavelength division multiplexer (WDM). An isolator with an isolation of 38 dB at a wavelength of 1.85 μm removes any unwanted back propagation light from the loop. A 95%:5% coupler provides 5% of the power to an OSA. Both ends of As_2S_3 fibers are butt-coupled to silica fibers via UV-cured epoxies. The relatively high pump power needed to reach lasing threshold is attributed to insertion losses of the optical components at a wavelength of 1.85 μm including $\sim$4 dB for isolator, $\sim$10 dB for chalcogenide FFP-TF and $\sim$5 dB for UV-cured epoxy connections and $\sim$1.5 dB for silica fiber. The laser wavelength is controlled by the FFP-TF.

Figure 8 illustrates the laser spectra tuned from 1.835 μm to 1.920 μm with a resolution of 1 nm. The demonstrated tunability is limited by the gain spectrum of Tm.

V. Conclusion

In conclusion, we have demonstrated the first all-fiber Fabry-Perot tunable filter compatible with the MIR range. Thin-film coating structures that consists of alternate layers of CaF_2 and Ge were successfully assembled, showing mechanical stability and compatibility with mid-infrared device fabrication. In tandem with this type of FFP-TF, truly MIR tunable lasers can be fabricated with suitable rare-earth gain medium or nonlinear processes such as four-wave mixing.

References

[1] G. Budinova, J. Salva, and K. Volka, "Application of molecular spectroscopy in the mid-infrared region to the determination of glucose and cholesterol in whole blood and in blood serum," *Appl. Spectrosc.*, vol. 51, no. 5, pp. 631–635, May 1997.

[2] B. H. Stuart, *Infrared Spectroscopy: Fundamentals and Applications*. Chichester, U.K.: Wiley, 2004, chs. 4–7.

[3] J. H. Taylor and H. W. Yates, "Atmospheric transmission in the infrared," *J. Opt. Soc. Amer.*, vol. 47, no. 3, pp. 223–226, Mar. 1957.

[4] M. A. Mackanos *et al.*, "Pulse-duration-dependent mid-infrared laser ablation for biological applications," *IEEE J. Sel. Topics Quantum Electron.*, vol. 18, no. 4, pp. 1514–1522, Jul. 2012.

[5] J. Geng, Q. Wang, J. Wang, S. Jiang, and K. Hsu, "All-fiber wavelength-swept laser near 2 μm," *Opt. Lett.*, vol. 36, no. 19, pp. 3771–3773, Oct. 2011.

[6] K. J. Lee, I.-K. Hwang, H. C. Park, and B. Y. Kim, "Polarization-independent all-fiber acousto-optic tunable filter using torsional acoustic wave," *IEEE Photon. Technol. Lett.*, vol. 22, no. 8, pp. 523–525, Apr. 15, 2015.

[7] G. Bharathan, R. I. Woodward, M. Ams, D. D. Hudson, S. D. Jackson, and A. Fuerbach, "Direct inscription of Bragg gratings into coated fluoride fibers for widely tunable and robust mid-infrared lasers," *Opt. Express*, vol. 25, no. 24, pp. 30013–30019, Nov. 2017.

[8] V. S. Shiryaev and M. F. Churbanov, "Trends and prospects for development of chalcogenide fibers for mid-infrared transmission," *J. Non-Crystalline Solids*, vol. 377, pp. 225–230, Oct. 2013.

[9] J. S. Sanghera, L. B. Shaw, and I. D. Aggarwal, "Applications of chalcogenide glass optical fibers," *Comp. Rendus Chimie*, vol. 5, no. 12, pp. 873–883, Dec. 2002.

[10] W. H. Kim *et al.*, "Recent progress in chalcogenide fiber technology at NRL," *J. Non-Crystalline Solids*, vol. 431, pp. 8–15, Jan. 2016.

[11] F. Tavakoli, A. Rekik, and M. Rochette, "Broadband and wavelength-dependent chalcogenide optical fiber couplers," *IEEE Photon. Technol. Lett.*, vol. 29, no. 9, pp. 735–738, May 1, 2017.

[12] D. D. Hudson *et al.*, "Toward all-fiber supercontinuum spanning the mid-infrared," *Optica*, vol. 4, no. 10, pp. 1163–1166, Oct. 2017.

[13] A. Al-kadry, M. E. Amraoui, Y. Messaddeq, and M. Rochette, "Two octaves mid-infrared supercontinuum generation in As_2Se_3 microwires," *Opt. Express*, vol. 22, no. 25, pp. 31131–31137, Dec. 2014.

[14] R. Ahmad and M. Rochette, "All-chalcogenide Raman-parametric laser, wavelength converter, and amplifier in a single microwire," *IEEE J. Sel. Topics Quantum Electron.*, vol. 20, no. 5, pp. 299–304, Sep. 2014.

[15] R. Ahmad and M. Rochette, "High efficiency and ultra broadband optical parametric four-wave mixing in chalcogenide-PMMA hybrid microwires," *Opt. Express*, vol. 20, no. 9, pp. 9572–9580, Apr. 2012.

[16] I. C. M. Littler, L. B. Fu, E. C. Mägi, D. Pudo, and B. J. Eggleton, "Widely tunable, acousto-optic resonances in chalcogenide As_2Se_3 fiber," *Opt. Express*, vol. 14, no. 18, pp. 8088–8095, Sep. 2006.

[17] R. Ahmad and M. Rochette, "Photosensitivity at 1550 nm and Bragg grating inscription in As_2Se_3 chalcogenide microwires," *Appl. Phys. Lett.*, vol. 99, no. 6, pp. 061109–061112, Aug. 2011.

[18] H. A. Macleod, *Thin-Film Optical Filters*. Boca Raton, FL, USA: CRC Press, 2010, pp. 551–561.

[19] H. H. Li, "Refractive index of silicon and germanium and its wavelength and temperature derivatives," *J. Phys. Chem. Ref. Data*, vol. 9, no. 3, pp. 561–658, Jul. 1980.

[20] A. E. Ennos, "Stresses developed in optical film coatings," *Appl. Opt.*, vol. 5, no. 1, pp. 51–61, Jan. 1966.

[21] A. Ciesielski, L. Skowronski, W. Pacuski, and T. Szoplik, "Permittivity of Ge, Te and Se thin films in the 200–1500 nm spectral range. Predicting the segregation effects in silver," *Mater. Sci. Semicond. Process.*, vol. 81, pp. 64–67, Jul. 2018.

[22] O. S. Heavens and S. D. Smith, "Dielectric thin films," *J. Opt. Soc. Amer.*, vol. 47, no. 6, pp. 469–472, Jun. 1957.

[23] N. S. Gluck, H. Sankur, and W. J. Gunning, "Ion-assisted laser deposition of CaF_2 thin films at low temperatures," *J. Vac. Sci. Technol. A, Vac., Surf., Films*, vol. 7, no. 5, pp. 2983–2987, Sep. 1989.

[24] M. Bass, E. W. V. Stryland, D. R. Williams, and W. L. Wolfe, *Handbook of Optics: Fundamentals, Techniques and Design*. New York, NY, USA: McGraw-Hill, 1995, pp. 42–44.

[25] C. K. Carniglia and D. G. Jensen, "Single-layer model for surface roughness," *Appl. Opt.*, vol. 41, no. 16, pp. 3167–3171, 2002.

[26] Y. Jiang and C. Tang, "High-finesse microlens optical fiber Fabry-Perot filters," *Microw. Opt. Technol. Lett.*, vol. 50, no. 9, pp. 2386–2389, Sep. 2008.

[27] R. St-Gelais, A. Poulin, and Y.-A. Peter, "Advances in modeling, design, and fabrication of deep-etched multilayer resonators," *J. Lightw. Technol.*, vol. 30, no. 12, pp. 1900–1908, Jun. 15, 2012.